Journal of
Synchrotron
Radiation

ISSN 0909-0495

Received 2 October 2006
Accepted 22 November 2006

A sagittally focusing double-multilayer monochromator for ultrafast X-ray imaging applications

Yujie Wang,* Suresh Narayanan,* Jinyuan Liu,‡ Deming Shu, Ali Mashayekhi, Jun Qian and Jin Wang

Advanced Photon Source, Argonne National Laboratory, 9700 South Cass Avenue, Argonne, IL 60439, USA. E-mail: yujie@aps.anl.gov, sureshn@aps.anl.gov

The development of a sagittally focusing double-multilayer monochromator is reported, which produces a spatially extended wide-bandpass X-ray beam from an intense synchrotron bending-magnet source at the Advanced Photon Source, for ultrafast X-ray radiography and tomography applications. This monochromator consists of two W/B_4C multilayers with a 25 Å period coated on Si single-crystal substrates. The second multilayer is mounted on a sagittally focusing bender, which can dynamically change the bending radius of the multilayer in order to condense and focus the beam to various points along the beamline. With this new apparatus, it becomes possible to adjust the X-ray beam size to best match the area detector size and the object size to facilitate more efficient data collection using ultrafast X-ray radiography and tomography.

Keywords: X-ray optics; sagittally focusing double-multilayer monochromator; X-ray radiography.

1. Introduction

X-ray radiography and tomography are powerful X-ray diagnostic tools with a wide range of applications. Both techniques are based on the fact that an X-ray beam will be absorbed when it passes through matter. In reality, most X-ray samples have finite spatial dimensions. Therefore, to facilitate the data collection process, it is desirable to have an X-ray beam with a similar or slightly larger size than the sample while possessing sufficient spatial uniformity and brightness. A typical end-station at a third-generation synchrotron source, such as the Advanced Photon Source (APS), is normally more than 50 m away from the source. An X-ray beam using a 3 mrad horizontal aperture from a bending-magnet (BM) source can be wider than 150 mm in the horizontal direction. Such an X-ray beam would be too large for ultrafast two-dimensional X-ray detectors (Barna *et al.*, 1997) and samples. Also, the flux density would be greatly reduced without any focusing. This requirement prompts us to develop a monochromator with the condensing and focusing capability to produce a spatially extended wide-bandpass X-ray beam for ultrafast X-ray radiography and tomography applications. The development of the sagittally focusing multilayer monochromator is important for a wide variety of applications. For example, with brilliant synchrotron X-ray sources, microsecond time-resolved temporal resolution has already been achieved to elucidate the detailed three-dimensional structure and dynamics of high-pressure high-speed fuel sprays in the near-nozzle region (MacPhee *et al.*, 2002; Cai *et al.*, 2003; Liu *et al.*, 2006). To optimize the data collection process, we must be able to manipulate the X-ray beam to deliver the ideal shape and size. However, an X-ray beam cannot easily be focused by simple lenses due to its weak interaction with matter; as a result, much more complex schemes have to be conceived. Over the years, various efforts for focusing X-ray beams have been carried out, including compound lenses (Snigirev *et al.*, 1996), zone plates (Yun *et al.*, 1999), capillary optics (Thiel *et al.*, 1993; Bilderback & Thiel, 1995), grazing-incidence toroidal mirrors (Sakayanagi & Aoki, 1978), KB mirrors (Kirkpatrick & Baez, 1948) and graded multilayer optics (Morawe *et al.*, 1999) *etc.*

These approaches in focusing the X-ray beam have also been considered in our design process, but they are less suitable for our experimental needs. Capillary-based optics cannot deliver the energy resolution required for quantitative measurements. Although preformed multilayers with a fixed sagittal radius can deliver the correct beam shape (Headrick *et al.*, 2002), they can only be used for fixed-energy applications since the optimal sagittal-focusing radius varies with energy. The meridional focusing concept is less suitable when the incoming beam divergence is large, and the physical dimension of the optics will be impractically large in order to intercept the whole beam.

In this work we report the development of the first dynamical sagittally focusing multilayer monochromator. This monochromator combines multilayer optics and the sagittal-focusing concept to deliver a high-brightness spatially extended X-ray beam whose size is dynamically adjustable.

‡ Current address: Institute of Optoelectronics, Shenzhen University, Shenzhen 518060, People's Republic of China.

Application of the sagittal-focusing concept in monochromator design can be traced back to the 1980s (Sparks *et al.*, 1982; Mills *et al.*, 1986). The wide-fan X-ray beams generated from BM sources were focused using sagittal bending. The sagittal radius of the crystal can be dynamically changed, and the X-rays can be focused to adjustable downstream distances.

Multilayer monochromators have been widely used in applications where the energy resolution requirement is less stringent (Stephenson, 1988; Chu *et al.*, 2002; Bigault *et al.*, 2003). In these situations, multilayers instead of crystal optics can be used to deliver a brighter X-ray beam with reasonable energy bandwidth. However, most existing multilayer monochromators lack focusing capabilities.

Substantial difficulties exist in applying multilayer optics in the sagittal-focusing geometry, however. Multilayers have larger interlayer spacing than crystals do, resulting in much smaller Bragg reflection angles. Therefore, when used for focusing applications, the focusing performance of the multilayers is susceptible to small surface profile aberrations. This drawback is aggravated when the sagittal-focusing technique is affected by anticlastic bending. This originates from the fact that, compared with a crystal, a much smaller sagittal radius is required for a multilayer to focus the same divergent X-ray beam; thus, only a very thin substrate can be used. The sagittal radius required to focus the X-ray is given by

$$r = [2pq/(p+q)]\sin\theta_{\rm B}, \qquad (1)$$

where p is the source-to-monochromator distance, q is the monochromator-to-focus distance and $\theta_{\rm B}$ is the Bragg angle. The anticlastic radius is proportional to the bending radius (Krisch *et al.*, 1991), $r_{\rm anti} = r/\sigma$ (σ is Poisson's ratio), and for multilayers the sagittal bending radius is in the sub-metre range. Therefore, in the sagittal-focusing geometry, maintaining the parallelism of the two monochromator multilayer surfaces will be difficult.

One of the methods of mitigating the effect of anticlastic bending has been strengthening the back of the crystal with stiffening ribs (Sparks *et al.*, 1982; Batterman & Berman, 1983; Pascarelli *et al.*, 1996; Freund *et al.*, 1996). However, even though this scheme can well compensate the anticlastic bending at the focal spot, it will generate a complex beam microstructure at non-focusing planes, which renders it ineffective for imaging applications. In this work we decided to use the 'golden ratio' method to reduce the anticlastic bending effect without introducing a complex structure into the beam (Kushnir *et al.*, 1993).

2. Monochromator design

2.1. Optical aspects

To be capable of intercepting a large portion of X-rays from a BM source, the monochromator consists of two large W/B_4C multilayers coated on Si single-crystal substrates with extended dimensions 90 mm long (L) × 90 mm wide (W) × 15 mm thick (T) for the first substrate and 120 mm (L) × 90 mm (W) × 2 mm (T) for the second. The sizes were chosen to fit on an existing commercial bender manufactured by Kohzu Inc. (Yoneda *et al.*, 2001). As shown in Fig. 1, both Si substrates have (111) orientation and were polished (at Waveprecision Inc.) to an optically measured root-mean-square (r.m.s.) surface roughness of around 0.5 Å. The polished substrates were deposited with W/B_4C multilayers (at Osmic Inc.) consisting of 100 periods of double layers, with each double layer having a thickness of 24.25 ± 0.25 Å. The surface was coated with a 28 Å B_4C cap layer to protect the W sublayers underneath from oxidization. The W/B_4C multilayers were chosen for their electron density contrast and thermal stability at high-heat load (Headrick *et al.*, 2002; Ziegler, 1995). In addition, uniformly thick W/B_4C layers can be deposited. The thickness ratio between the W and B_4C layers was chosen to be 0.5 to suppress the second harmonic reflection. The second silicon substrate started with a silicon (111) slab with dimensions 120 mm × 90 mm × 2 mm. Subsequently, the central part of the crystal was thinned down to 0.5 mm, while the wings were kept at their original thickness. The crystal was designed such that the thin part has an aspect ratio of 1.42 between the meridional and sagittal directions to reduce the unwanted anticlastic bending as discussed before (Kushnir *et al.*, 1993). By testing different aspect ratios with both Si (100) and (111) substrates, the golden ratio was indeed proven to be 1.42 for both crystalline orientations by optical metrology.

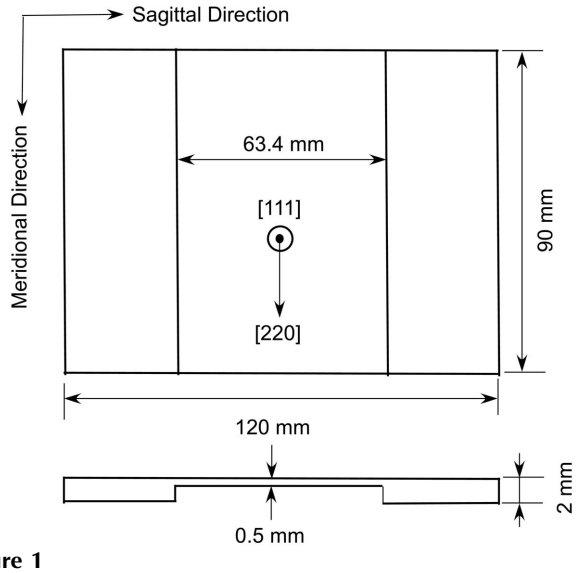

Figure 1
Schematic of the sagittal-focusing multilayer substrate. The substrate is prepared from a Si (111) slab. The central thin portion maintains the golden aspect ratio of 1.42 (90:63.4). The multilayer is deposited on the flat side. The thick wings were clamped to the bender. The bender can dynamically change the sagittal radius of the crystal by introducing a bending load. The resulting cylindrical-shaped surface can focus the reflecting X-ray beam horizontally.

2.2. Mechanical aspects

The crystals are mounted on two independent, motorized and high-precision Kohzu stage groups to allow X-ray energy

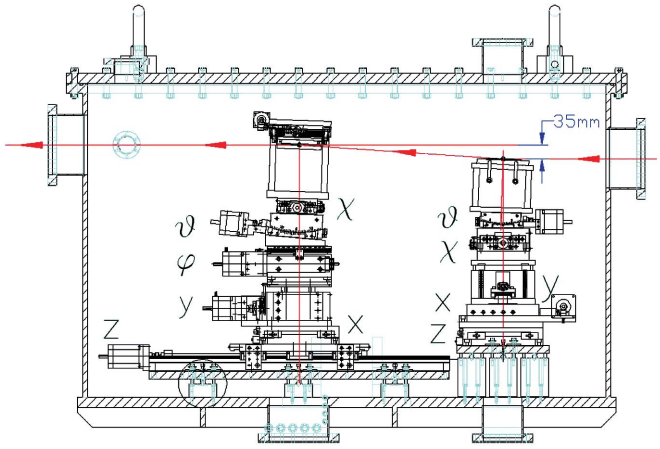

Figure 2
Schematic of the high-vacuum chamber and vacuum-compatible high-precision motorized stages. The collimated X-ray beam from beamline 1-BM enters the chamber from the right-hand port, and the subsequent monochromatic X-rays exit the chamber from the left-hand vacuum port with a vertical offset of 35 mm. The vertical offset can be adjusted by changing the second multilayer element height.

selection from 5 to 10 keV. A 35 mm vertical offset between the two multilayers was chosen to maintain the ray tracing of the existing beamline (Lang *et al.*, 1999). This large offset will guarantee that the multilayer can match that for the previously existing double-crystal monochromator. The energy selection and alignment of the two crystals are accomplished by the 11 high-precision motorized translation and rotary stages (Fig. 2). The stages for the first multilayer element has x, y, z, θ and χ motions and that for the second element has x, y, z, θ, φ and χ motors. The χ and φ motions are necessary for alignment of both elements with respect to the X-ray beam axis. To avoid ozone generation and oxidization of the multilayers, the entire system is housed in a large high-vacuum chamber (1500 mm × 800 mm × 600 mm) at 10^{-7} mbar. To mitigate the high-heat-load problem that could induce thermal interlayer diffusion in the first multilayer element, the first multilayer element is water-cooled by direct thermal contact with a copper cooling block. The cooling water was supplied by a gravity-feed system to isolate vibrations from mechanical water pumps.

3. Results and discussion

The X-ray reflectivity for both multilayer elements was measured at 8 keV at beamline 1-BM of the APS before the crystals were installed in the high-vacuum chamber. One of the multilayers was also measured at 7.35 keV at the 8-ID beamline to obtain the absolute value of the reflectivity at the first Bragg peak. The reflectivity curve on a logarithmic scale is shown in Fig. 3. The experimentally measured reflectivity curve is compared with theoretical simulation. In inset (*a*) of Fig. 3 the curve on a linear scale shows that the reflectivity is 68% at this energy at the first Bragg reflection, which confirms the superior coating quality. The second and third harmonic reflectivity is less than 0.3%, thus, with reflection from both

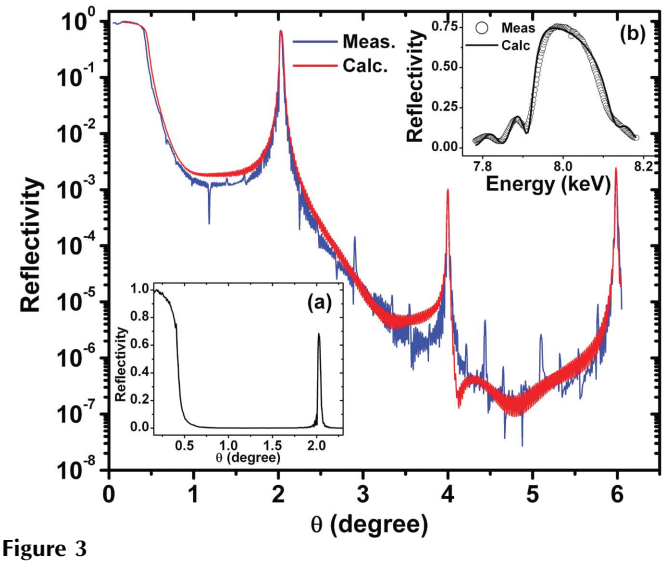

Figure 3
Normalized reflectivity measured at 7.35 keV from the first multilayer crystal. The insets show the reflectivity data in a linear scale (*a*) and the rocking curve when the crystal is oriented at the first Bragg angle (*b*). The reflectivity at the first Bragg angle is 68% at 7.35 keV as the energy bandwidth is calculated to be 2% at 8 keV.

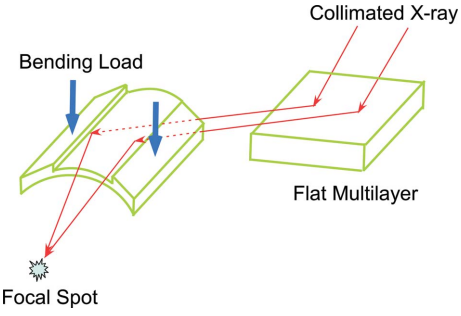

Figure 4
Schematic of the scattering geometry of the monochromator. The incoming collimated X-ray beam is reflected from the first multilayer at the Bragg angle. The second crystal is located downstream and has a 35 mm fixed vertical offset from the first crystal. The reflected beam is intercepted by the second multilayer also at the Bragg angle.

multilayers, the second and third harmonic reflectivity is less than 9×10^{-6} of the first harmonic reflectivity. As a result, at 7.35 keV, for most applications, in principle no additional mirror is needed to reject the high-order harmonic reflection contaminations. In inset (*b*) of Fig. 3, a rocking-curve scan at the first Bragg reflection angle at 8 keV shows a full width at half-maximum (FWHM) of 150 eV, so the monochromator bandwidth is around 2%. The reflectivity and energy scans match well with our theoretical simulations.

The existing optics at the 1-BM beamline of APS includes an upstream collimating mirror (20 m from the source) and a downstream vertical-focusing mirror (40 m from the source). This multilayer monochromator is installed 36 m from the source. By moving the existing double-crystal monochromator and the downstream focusing mirror out of the X-ray beam path, we measured the performance of the multilayer monochromator using the collimated beam from the upstream collimating mirror. The scattering geometry is shown in Fig. 4.

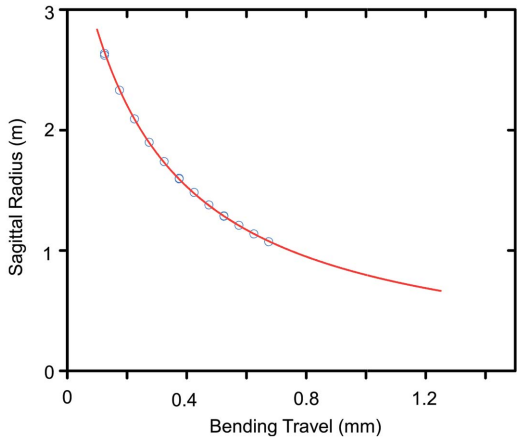

Figure 5
Bending characteristics of the sagittal multilayer element mounted on a Kohzu bender from optical metrology measurements. The optical metrology measurement can only measure radii up to ~1 m; the data were extrapolated to the sub-metre range by an inverse polynomial fitting.

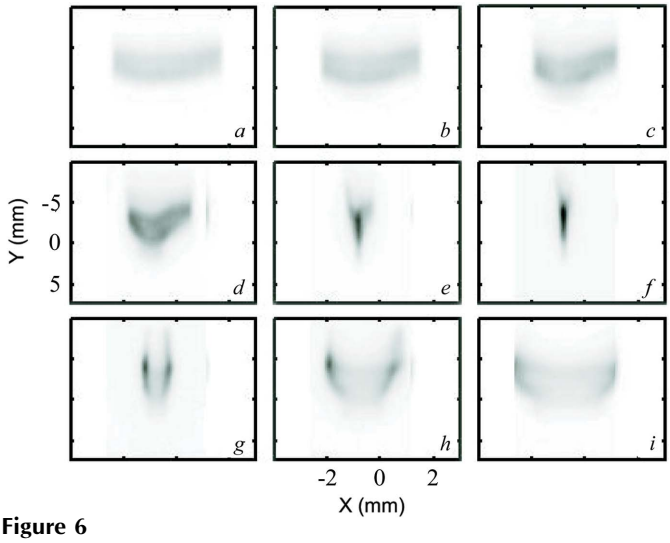

Figure 6
X-ray beam shape in the end-station imaged by a CCD camera while the bender dynamically changes the bending radius of the sagittal crystal, in turn, the focal distance. The images correspond to under-focus (*a*–*e*), focus (*f*) and over-focus (*g*–*i*) bending conditions.

To focus the X-ray beam in the range from 6 to 9 keV to the end-station located 53 m from the source, a variable sagittal radius from 0.9 to 0.5 m is needed; the necessary bending displacements have been calibrated in advance also by optical long-trace-profiler (LTP) measurements as shown in Fig. 5.

Fig. 6 shows the focused X-ray beam at 8 keV imaged by a Roper Scientific Coolsnap HQ X-ray CCD camera at the end-station with various sagittal bending radii, illustrating the evolution of the beam when the sagittal crystal is bent from under-focus to over-focus conditions. The CCD camera has 1024 × 1280 pixels with a pixel size of 6.67 μm × 6.67 μm. The X-ray beam is converted to visible light using a YAG:Ce scintillator and collected by an optical lens of 1× magnification. As shown in Fig. 6, the smallest focal spot is 0.35 mm (FWHM) in the horizontal direction when no vertical focusing optics is used. The vertical beam size of 1.28 mm (FWHM) is close to the value of the vertical beam size intercepted by the multilayer. When the monochromator is used for delivering an intense X-ray beam with an extended and adjustable beam size, the overall performance of the monochromator can be characterized by its total flux and the maximum uniform beam size. For time-resolved tomography and radiography experiments, a beam size of the order of several millimetres to centimetres in the horizontal direction with high and uniform intensity is required. Both criteria are well met with this monochromator. We measured that the maximum X-ray flux that can be delivered by the monochromator is around 1.4×10^{13} photons s^{-1} at 8 keV. This flux is about 20 times higher than the flux delivered by a sagittal-focusing Si (111) crystal monochromator at the same APS beamline (Lang *et al.*, 1999). Additionally, a fairly uniform and square-shaped beam can be delivered when the multilayer is in an under- or over-focus condition, as illustrated in Fig. 6. Theoretically, the gain of about 100 in the flux is expected over Si (111) crystals due to the increase in energy bandwidth for a multilayer monochromator. Because the reflectivity from the multilayer is significantly less than unity, and the low Bragg angle of the multilayer intercepts a smaller vertical beam, a flux gain of around 40 times is expected. The actual loss in the intensity is attributed primarily to optical aberrations and will be discussed in detail in the following sections.

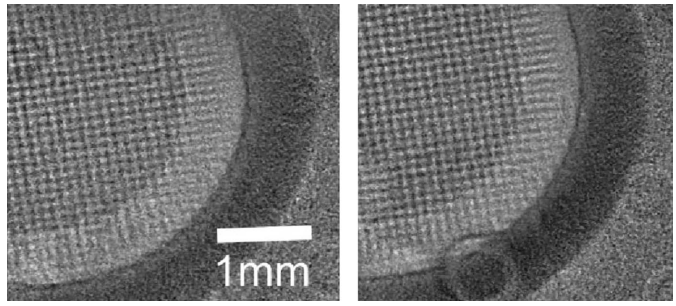

Figure 7
Images of gold mesh standard (300 lines $inch^{-1}$) when the CCD camera was placed 3 mm (left) and 100 mm (right, representing a more realistic sample–detector distance) away.

Since the monochromator is designed for imaging purposes, we also calibrated the near-field fidelity of the imaging system. We have imaged a gold mesh standard (300 lines $inch^{-1}$) as shown in Fig. 7 by positioning the CCD camera 3 and 100 mm away. Detailed calculations comparing the sizes of the same mesh grid revealed that certain horizontal divergence of the beam exists, which can causes around 1% magnification or demagnification depending on the relative position of the object to the X-ray focal point, in the 100 mm travel range.

The performance of the monochromator has left some room for improvement. One important aspect is understanding the origin of the aberrations in the X-ray beam shape. To achieve this goal, we have compared our optical metrology results of the monochromator crystal surface profile with the corresponding X-ray image shape. The optical metrology study was carried out before the multilayer element was mounted.

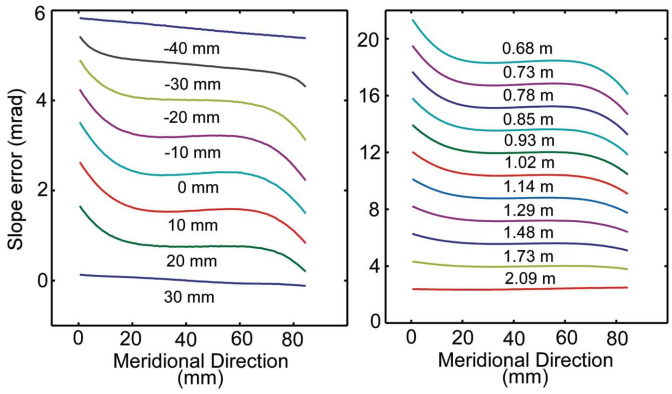

Figure 8
Surface slope error of the sagittal substrate under bending along the meridional direction by optical LTP at a sagittal radius of 1.14 m (left-hand panel) and of the centreline along the meridional direction with various sagittal radii (right-hand panel). The curves in both panels have no slope error in the centre and are offset for clarity.

Optical metrology has been routinely used to characterize the surface aberrations of X-ray optics surfaces. To optimize the crystal design based on the bender made by Kohzu, we carried out substantial optical metrology studies of the bending characteristics of the substrates. In the left-hand panel of Fig. 8, the surface slope error of the substrate crystal under sagittal bending load (sagittal radius = 1.14 m) was plotted along several lines along the meridional direction of the surface. There exists a flat region in the centre of the crystal surface (about 40 mm) along the meridional direction. The substrate develops serious twisting and curvature when approaching the edge along both the sagittal and meridional directions. In the right-hand panel of Fig. 8, the surface slope error along the centreline of the meridional direction of the substrate is plotted with increasing bending load. Obviously, direct correlation exists between the decreasing bending radius and the aberration.

Along the sagittal direction, we have also observed a gradual change in the bending radius towards the edges of the substrate. This aberration was naturally attributed to the existence of the thick wings since the thicker wings yield less under the same bending load; thus this deviation in the bending radius will change the surface profile from the ideal cylindrical shape for ideal focusing.

To correlate the X-ray beam shape with the optical metrology results, we performed X-ray metrology studies of the combined performance of the multilayers. The imaging conditions are chosen to be the same as those in Fig. 6 when the sagittal substrate was bent to 1 m sagittal radius and the multilayer was set to be at the Bragg condition at 8 keV. To understand the beam profile contribution from each part of the sagittal multilayer (assuming the aberration only originates from the sagittal multilayer), we used a small X-ray beam in the vertical direction to scan through the multilayer surfaces. In Fig. 9 (top panels), a vertical 0.1 mm-size X-ray beam (horizontally wide open) was used to scan the crystal surface vertically and the reflected X-ray beam was recorded using the CCD camera. The images were recorded at each

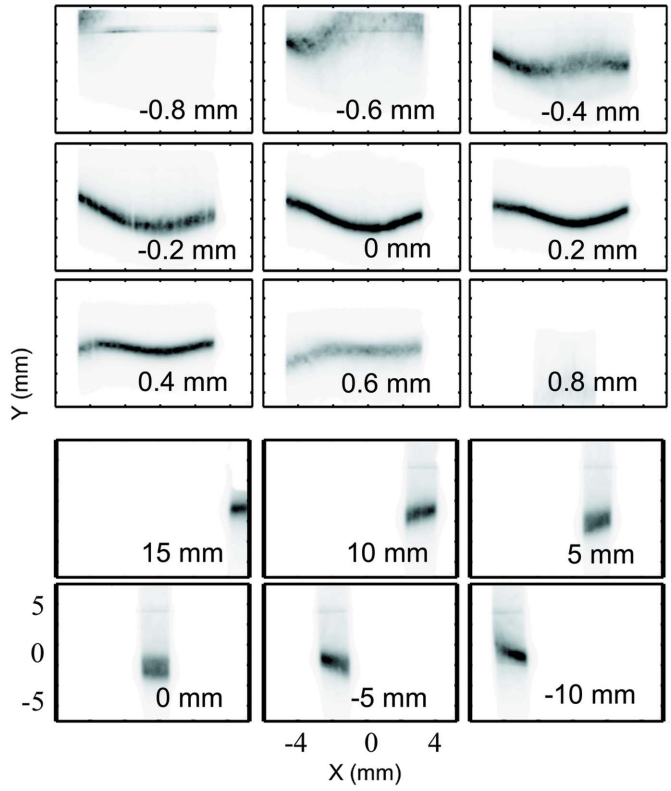

Figure 9
X-ray metrology study of the sagittal substrate surface profile when it is bent to a sagittal radius of 1 m. The substrate was oriented to intercept the incoming X-ray beam at the Bragg angle. The upper nine panels show the X-ray beam shape in the end-station when an X-ray beam with 0.1 mm vertical size is scanned through the surface vertically. The lower six panels show the X-ray beam shape when an X-ray slit of 5 mm horizontal size is scanned through the surface horizontally.

0.2 mm step. The multilayer is supposed to intercept 2.8 mm of the vertical beam. However, owing to the anticlastic bending, the boundary portion of the substrate along the meridional direction does not satisfy Bragg's law (the multilayer rocking-curve width at 8 keV is around 0.87 mrad), thus the substrate can only intercept around 1.6 mm of the vertical beam, as shown in the top panels of Fig. 9; this is in agreement with our optical metrology study. Even the X-ray image formed by reflection from the centre of the substrate has a non-square shape. To further understand these aberrations, a horizontal 5 mm beam (vertically wide open) was used to scan the surface horizontally. The images were recorded at a horizontal step of 5 mm. The central portion of the substrate can clearly contribute to a square-shaped image, while it deviates from the square-shape as the beam moves to the wings, which is a strong indication of the non-uniformity of the sagittal radius along the sagittal direction. Again, the X-ray metrology results confirm the optical metrology results well. As a result, we can identify that most of the aberrations come from the areas near the wings of the substrates. Based on both the X-ray and optical metrology, the aberrations can be possibly reduced by using a much larger crystal substrate (and correspondingly a larger bender). In this case the X-ray beam only impinges on the flat centre portion of the multilayer element.

4. Conclusions

To summarize, the dynamically sagittal-focusing multilayer monochromator can deliver substantially higher flux as compared with a crystal monochromator. Additionally, by dynamically changing the sagittal bending radius, an X-ray beam with an adjustable horizontal size can be delivered, which is crucial for X-ray radiography or tomography to match the sample and detector sizes. With high flux, the development of the new dynamic sagittal-focusing monochromator will offer new opportunities in time-resolved imaging experiments.

However, because of the large degree of bending, the aberrations can be severe, as observed by both optical and X-ray metrology. The aberrations will have inadvertent effects on imaging applications in the far field. In the near field, the image distortion due to the aberrations can be negligible. Therefore, this monochromator can be effective for proposed radiographic and tomographic experiments where only near-field imaging is required.

We would like to thank Dean Haeffner and Roger Ranay at Sector 1 and Xuefa Li of Sector 8 of the APS for support. Also, Ruben Khachatrayan helped with the substrate manufacturing. We also thank Eric Dufresne for critical comments. This work was supported by the Office of FreedomCAR and Vehicle Technology Program of the US Department Energy (DoE) and the use of the APS was supported by the US DoE, Office of Science, Office of Basic Energy Sciences, under Contract No. DE-AC02-06CH11357.

References

Barna, S. L., Shepherd, J. A., Tate, M. W., Wixted, R. L., Eikenberry, E. F. & Gruner, S. M. (1997). *IEEE Trans. Nucl. Sci.* **44**, 950–956.
Batterman, W. & Berman, L. (1983). *Nucl. Instrum. Methods*, **208**, 327–331.
Bigault, T., Ziegler, E., Morawe, C., Hustache, R., Massonnat, J. Y. & Rostaing, G. (2003). *Proc. SPIE*, **1775**, 12–20.
Bilderback, D. H. & Thiel, D. J. (1995). *Rev. Sci. Instrum.* **66**, 2059–2063.
Cai, W. Y., Powell, C. F., Yue, Y., Narayanan, S., Wang, J., Tate, M. W., Renzi, M. J., Ercan, A., Fontes, E. & Gruner, S. M. (2003). *Appl. Phys. Lett.* **83**, 1671–1673.
Chu, Y. S., Liu, C., Mancini, D. C., De Carlo, F., Macrander, A. T., Lai, B. & Shu, D. (2002). *Rev. Sci. Instrum.* **73**, 1485–1487.
Freund, A. K., Comin, F., Hazemann, J. L., Hustache, R., Jenninger, B., Lieb, K. & Pierre, M. (1996). *Proc. SPIE*, **3448**, 144–155.
Headrick, R. L., Smolenski, K. W., Kazimirov, A., Liu, C. & Macrander, A. T. (2002). *Rev. Sci. Instrum.* **73**, 1476–1479.
Kirkpatrick, P. & Baez, A. V. (1948). *J. Opt. Soc. Am.* **38**, 766–774.
Krisch, M., Freund, A., Marot, G. & Zhang, L. (1991). *Nucl. Instrum. Methods*, A**305**, 208–213.
Kushnir, V. I., Quintata, J. P. & Georgopoulos, P. (1993). *Nucl. Instrum. Mechods*, A**328**, 588–591.
Lang, L. C., Srajer, G., Wang, J. & Lee, P. L. (1999). *Rev. Sci. Instrum.* **70**, 4457–4462.
Liu, X. *et al.* (2006). *SAE Trans.* 2006-01-1041.
MacPhee, A. G., Tate, M. W., Powell, C. F., Yue, Y., Renzi, M. J., Ercan, A., Narayanan, S., Fontes, E., Walther, J., Schaller, J., Gruner, S. M. & Wang, J. (2002). *Science*, **295**, 1261–1263.
Mills, D. M., Henderson, C. & Batterman, B. W. (1986). *Nucl. Instrum. Methods*, A**246**, 356–359.
Morawe, C., Pecci, P., Peffen, J. C. & Ziegler, E. (1999). *Rev. Sci. Instrum.* **70**, 3227–3232.
Pascarelli, S., Boscherini, F., D'Acapito, F., Hrdy, J., Meneghini, C. & Mobilio, S. (1996). *J. Synchrotron Rad.* **3**, 147–155.
Sakayanagi, Y. & Aoki, S. (1978). *Appl. Opt.* **17**, 601–603.
Snigirev, A., Kohn, V., Snigireva, I. & Lengeler, B. (1996). *Nature (London)*, **384**, 49–51.
Sparks, C. J., Ice, G. E., Wong, J. & Batterman, B. M. (1982). *Nucl. Instrum. Methods*, **194**, 73–78.
Stephenson, G. B. (1988). *Nucl. Instrum. Methods*, A**266**, 447–451.
Thiel, D. J., Bilderback, D. H. & Lewis, A. (1993). *Rev. Sci. Instrum.* **64**, 2872–2878.
Yoneda, Y., Matsumoto, N., Furukawa, Y. & Ishikawa, T. (2001). *J. Synchrotron Rad.* **8**, 18–21.
Yun, W., Lai, B., Cai, Z. & Maser, J. (1999). *Rev. Sci. Instrum.* **70**, 2238–2241.
Ziegler, E. (1995). *Opt. Eng.* **34**, 445–452.